ACS Catalysis

Research Article

pubs.acs.org/acscatalysis

# Rutile-Deposited Pt−Pd clusters: A Hypothesis Regarding the Stability at 50/50 Ratio

Mai-Anh Ha,[†,§] Jonny Dadras,[†,§] and Anastassia Alexandrova*[,†,‡]

[†]Department of Chemistry and Biochemistry, University of California, 607 Charles E Young Drive East, Box 951569, Los Angeles, California 90095, United States

[‡]California NanoSystems Institute, 570 Westwood Plaza, Los Angeles, California 90095, United States

*Supporting Information*

**ABSTRACT:** Mixed Pt−Pd clusters deposited on oxides have been of great interest to catalysis. Clusters containing Pt and Pd in roughly equal proportions were found to be unusually stable against sintering, one of the major mechanisms of catalyst deactivation. After aging of such catalysts, the 50/50 Pt−Pd and Pd−O clusters appeared to be the two most prevalent phases. The reason for the enhanced stability of these equally proportioned clusters has remained unclear. In the following, sintering of mixed Pt−Pd clusters on $TiO_2(110)$ for various initial atomic concentrations of Pt and Pd and at a range of catalytically relevant temperatures was simulated. It is confirmed that equally mixed clusters have the relatively highest survival rate. Surprisingly, subnanoclusters containing Pt and Pd in all proportions have very similar geometries and chemical bonding, revealing no apparent explanation for favoring the 1:1 Pt/Pd ratio. However, it was discovered that at high temperatures, the 50/50 clusters have considerably more thermally accessible isomers than clusters containing Pt and Pd in other proportions. Hence, one of the reasons for stability is entropic stabilization. Electrostatics also plays a key role as a subtle charge redistribution, and a shift of electron density to the slightly more electronegative Pt results in the partially charged atoms being further stabilized by intracluster Coulomb attraction; this effect is greatest for 1:1 mixtures.

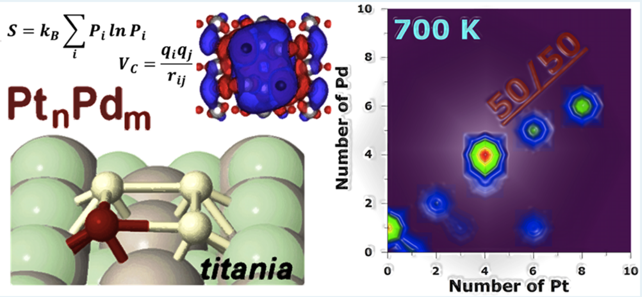

**KEYWORDS:** *PtPd clusters on titania, density functional theory, sintering, Monte Carlo, theory, chemical bonding*

## 1. INTRODUCTION

Supported Pt nanoclusters have shown great catalytic activity and selectivity for alkane dehydrogenation and cracking.[1−4] Recently, it has been shown that Pt and Pd on zeolite (ZSM-5) greatly increased these catalytic properties beyond that of ZSM-5 alone.[5,6] Additional dehydrogenation to alkynes can occur, as well as methane formation from cracking, and both of these can result in coke deposition. For dehydrogenation catalyzed by deposited clusters, two mechanisms for catalysis deactivation are the prime suspects: coke deposition and cluster sintering. Coke fouling reduces catalytic activity of the clusters, and therefore, a primary approach to reduce coking involves alloying Pt with main group metals, as well as some transition metals.[7−12] Gutierrez et al. have demonstrated that deactivation of Pt−Pd clusters resulting from deposited coke can be reduced by controlling the acidity of the support.[13] Sintering of metal nanoparticles is a result of the particles minimizing their surface energy; hence, populations of small sized particles decrease with a corresponding increase of large-sized particle populations. Graham et al. have shown that mixed Pt−Pd clusters, supported on alumina, have improved stability over those of just pure Pt.[14] However, Johns et al. showed conflicting results of the sintering rate of Pt−Pd nanoparticles.[15] It is noted that the latter study observed no core−shell structure of nanoparticles under conditions relevant for industrial applications, in contrast with results of, for example, Anderson et al. on smaller-sized (approximately 2 nm) bimetallic nanoparticles.[16] A proper understanding of the catalytic properties of these Pt−Pd bimetallic clusters as well as their structure, stability, and mobility requires deeper knowledge of this system at the nano and subnano scales.

For subnanoclusters, the role of the surface goes beyond that of a stage on which the action of catalysis is played. The rutile $TiO_2(110)$ is a popular model support of the transition metal−oxide interface, providing controllable surface conditions (e.g., adsorption sites) to study various catalytic reaction pathways.[17−19] Previously, one of the authors (Alexandrova) has shown that pure Pd clusters deposited on $TiO_2$ will readily sinter, by the Ostwald ripening mechanism,[20] greatly decreasing the catalytic activity of the clusters by reducing the number of edge or step sites. Ostwald ripening, as opposed to particle coalescence, is indeed the mechanism expected to be operational for Pt, Pd, and mixed Pt−Pd clusters on titania.[21]

**Received:** June 21, 2014
**Revised:** September 2, 2014
**Published:** September 4, 2014

In the present work, the process of sintering of mixed Pt−Pd clusters on titania via Ostwald ripening is tackled. To this end, our newly extended ab initio Metropolis Monte Carlo method and ab initio and PW-DFT are employed. Sintering at various initial conditions and several experimentally relevant temperatures is modeled, and our results agree with the experimental observations that claim the Pt−Pd clusters containing Pt and Pd in equal proportions are the most stable against sintering. Finally, the long-standing question of why these clusters exhibit special stability is addressed by an extensive chemical bonding analyses of the thermally relevant isomers of the studied systems; statistical mechanical arguments are also provided. A detailed and physically well-motivated hypothesis is presented to explain the puzzling and appealing stability of 1:1 mixtures of surface-supported Pt−Pd clusters.

## 2. COMPUTATIONAL METHODOLOGIES

**2.1. Electronic Structure Methods.** As was previously done,[20] all PW-DFT calculations were performed with the Quantum Espresso package using the most recently available ultrasoft pseudopotentials with scalar relativistic corrections,[22−25] and spin-unrestricted calculations were done employing the PBE functional.[26] Large kinetic energy cutoffs of 435.2 eV and 4.352 keV were applied to the wave functions and charge density, respectively. A 1 × 1 × 1 Monkhorst−Pack k-point grid was used for all calculations and shifts away from the gamma-point were applied in $x$ and $y$ in order to maintain good accuracy. The titania slab was modeled as a 4 × 2 unit cell with four-trilayers along $z$ with a lattice constant of $a = 4.67$ Å and $c = 3.02$ Å. A vacuum gap of about 13 Å between the top and bottom surface atoms of repeating images ensures errors in the energies are on the order of a few meV. The bottom two trilayers of titania were held fixed and—as encouraged by Kowalski et al.[27,28] to prevent spurious surface states and other effects—dangling bonds of Ti and O atoms were saturated with pseudohydrogens having charges of 4/3 e and 2/3 e, respectively.

For the clusters in the gas-phase, a variety of DFT and ab initio methods were employed to check the performance of PW-DFT for the studied systems. Geometries and relative energies of isomers were refined using the TPSS(h)[29] (hybrid) functional with the aug-cc-pVTZ-pp basis set.[30,31] Additionally, CASSCF(m,n)[32−37]/LANL2DZ[38−41] results were used to check the nature of the wave functions and the applicability of single-determinant methods. It was found that results across theoretical methods are in good agreement (presented in the Supporting Information (SI)) and also that the single-reference approximation is valid with the Hartree−Fock contribution to the CASSCF expansion being greater than 0.9 for all systems. All ab initio gas phase calculations were done using Gaussian 09.[42]

For the chemical bonding analysis, the Bader charge localization scheme for PW-DFT systems was used.[43−45] For gaseous clusters, NBO[46] at the TPSSh/aug-cc-pVTZ-pp level of theory was used. NPA charges were found to be in close agreement with Bader, for the clusters in the gas phase, and therefore, Bader charges were used for our arguments to be consistent with the methods used for surface-supported clusters. Molecular orbitals (MOs) were plotted using the postprocessing package provided with Quantum Espresso at the Γ-point. Results presented in the main text are based on PW-DFT.

**2.2. Monte Carlo Algorithm for Sintering.** In order to assess the evolution of cluster sizes and compositions at different temperatures and to illustrate how certain very small sizes are not stable enough to withstand elevated temperatures relevant to experiment, a Monte Carlo scheme was employed. The algorithm, first published in 2011,[20] was based on the original proposal of Metropolis et al.[47] and extended by Hastings.[48] Briefly, it is a Markov Chain Monte Carlo scheme sampling the canonical ensemble that seeks the configuration-space global minimum of monomers interacting with the support and forming clusters, via precomputed potential energy surfaces (PESs), that is, it models sintering by the Ostwald ripening mechanism. A monomer will, upon "collision," sinter to any multimer with unit probability. An atom is allowed to dissociate from a cluster forming a monomer and reduced cluster providing the Metropolis condition is satisfied:

$$\mathcal{P} = \min(1, \exp(-\beta E_s))$$

where $\beta$ is thermodynamic beta ($1/k_BT$, $k_B$ is Boltzmann's constant, and $T$ is the temperature) and $E_s$ is the sintering energy further discussed below.

In the present implementation, the original procedure is extended in several ways. First of all, it can handle bimetallic clusters (i.e. two separate PESs for the Pt and Pd monomers are used in simulations). The grid for the monomers' movement is made finer than in the original implementation, to better explore the PES. The so-called sintering energy $(E_s)^{20}$ is generalized to taking the energy difference ($\Delta E = E_f - E_i$) for the reaction

$$[\mathrm{Pt-Pd}]_j + [\mathrm{Pt-Pd}]_k \rightarrow [\mathrm{Pt-Pd}]_{j-1} + [\mathrm{Pt-Pd}]_{k+1}$$

where $j$ and $k$ are sums of the numbers of Pt and Pd atoms in a given cluster. Hence,

$$\Delta E = E[[\mathrm{Pt-Pd}]_{j-1}] + E[[\mathrm{Pt-Pd}]_{k+1}] - E[[\mathrm{Pt-Pd}]_j] - E[[\mathrm{Pt-Pd}]_k]$$

The energies here are given by the Boltzmann weighted average of the few most energetically favorable structures found by an extensive search (using PW-DFT) for the global and local minima of the given cluster type ($\mathrm{Pt}_m\mathrm{Pd}_n$) on titania—this is further explained in the following section. It is noted that the above equation reduces to the same expression for $E_s$ of ref 20 in the limiting case where there is only a single element and when the final configuration includes a monomer. The above also generalizes the second-order energy difference ($\Delta_2E$), a measure of cluster's relative stability (defined in e.g. Wei et al.),[49] as it appears as a special case where the initial configuration is two of the same cluster type. The algorithm uses the energies of the monomers, dimers, trimers, and tetramers; however, the sintering energies for the transition to higher multimers were assumed to be equal those of the transition from the monomer plus trimer to the tetramers containing Pt and Pd in the appropriate proportion. This approach was used in the past[20] and additionally justified recently in a joint theoretical and experimental paper by Addou et al.[50] The searches for global and local minima were done ad nauseam by sampling over the geometries of the clusters and the potential binding sites on the support.

Only the stoichiometric $\mathrm{TiO_2}(100)$ surface was considered, because it was known that d-electron-rich atoms with electronic configuration of $d^9$ or $d^{10}$, such as Pt and Pd, preferentially bind to stoichiometric oxides.[20,51,52] O vacancies are electron-rich defects, and even though there exists a minimum near the vacancy for Pd, approaching it requires surmounting a large barrier, and vacancies can help cluster dissociation.[20] It is noted that to correctly ensure an atom breaking away from a cluster and given that this model will tend to favor 2D irregular-shaped (i.e., filamentary) cluster growth, a cluster-size-dependent step size is enforced that represents a closed-form analytic expression of the average of the sizes of clusters that would form when optimally packing circles in circles,[53] squares,[54] and linear chains (see SI).

Evaporation of monomers is allowed for by applying a Metropolis-like algorithm to the Boltzmann-factor containing the adsorption energy of the monomer at the given location ($E_{\mathrm{ads}}$) scaled by some factor. Pt and Pd are quite insensitive to evaporation at the studied temperatures, to zeroth-order, and the scaling factor was treated as a free parameter ($\gamma$) that was adjusted between the ranges of 0.5—2.0 for several test cases. Hence, the criteria to accept an "evaporation move" is given by the following probability distribution:

$$\mathcal{P} = \min(1, \exp\beta(E_{\mathrm{ads}} - \gamma))$$

Monomer redeposition on the support is also allowed, and coverage dependence is implicitly included in the model, as monomers can only redeposit in an unoccupied region of the support.

$$\mathcal{P} = \min(1, \exp\beta(E_{\mathrm{ads}} + \gamma))$$

Evaporation was negligible for both species under the considered parameters; this is due to the fact that the binding energy for a monomer to the support is on the order of ~1 eV (shown in section 3), corresponding to a temperature of ~$10^4$ K. When the evaporation rate is not negligible, like in the case of Zn,[55,56] a more physically motivated model is required; this is the subject of a forthcoming publication. It is noted that the effect of direct atom evaporation from a supported cluster is ignored as the energy cost for such an event is several eV.

The effect of temperature in the MC is addressed in two ways: First, it impacts the Boltzmann-weighted populations of each cluster and thus determines the average energies used in the simulations that determine whether an atom changes its configurational state. Second, the Metropolis criterion for accepting new structures in the simulations is explicitly temperature dependent. Deficiencies of the model include the lack of $O_2$ and $H_2O$ in the simulations, which are present in small quantities even under vacuum, leading some Pd to be taken up by PdO clusters (the present results shift toward Pd-rich phases when compared to data from O-rich environments), as well as not permitting surface modification or reconstruction. Although the effective relative well depths of the PES change, depending on temperature, their relative locations do not. Other effects, such as vibrational excitations with rising temperature and potential electronic excitations are not included in the Monte Carlo. However, these limitations of the model did not prevent the method from reproducing the cluster-size distributions resembling those found in experiment.[20,50]

## 3. RESULTS AND DISCUSSION

The relevant clusters that define the parameters of the sintering MC will be discussed briefly. Only the tetramers will be highlighted—smaller clusters are presented in Figures S1 and S2 in the Supporting Information. In Figures 1 and 2, the global and low-energy local minima for $\mathrm{Pt}_m\mathrm{Pd}_n$ ($m$,$n$ = 0,..,4 and $m + n$ = 4) clusters in the gas phase and on $\mathrm{TiO}_2$(110) are shown. The calculated formation energies of the most stable gas phase clusters are listed in Table 1, and the calculated adsorption energies and sintering energy penalties of the global minima of supported clusters at varying ratios of Pd and Pt are listed in Tables 2. For the gas-phase clusters, calculations using a variety of correlated electronic structure methods, with different basis sets, were carried out using Gaussian 09. It was found that the relative energies and geometries of clusters are consistent across theoretical methods, justifying the use of the PW-DFT methodology. Discussion of coordination to rutile oxygen utilizes the following notation: bridging surface oxygen atoms are denoted $O_b$, and in-plane surface oxygen atoms are denoted $O_s$. See Figure 2 for visualization.

**3.1. Clusters in the Gas Phase.** In the gas phase, tetramers adopt tetrahedral structures with square planar and rhomboidal isomers being noncompetitive at the temperatures of interest. Total formation energies ($E_f$) were calculated by

$$E_{\mathrm{f}} = E_{\mathrm{cluster}} - N_{\mathrm{Pd}}E[\mathrm{Pd}_1] - N_{\mathrm{Pt}}E[\mathrm{Pt}_1]$$

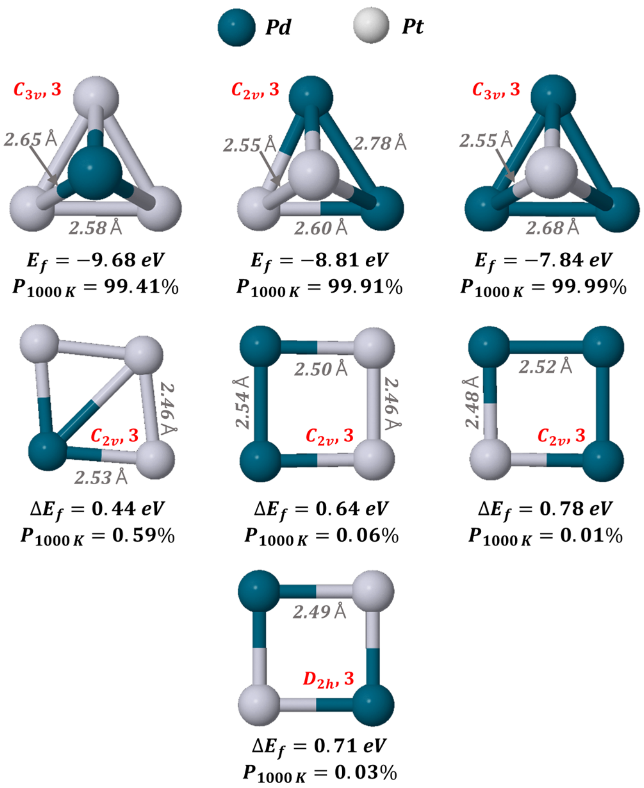

**Figure 1.** Most stable structures of the mixed clusters in the gas phase with their formation energies ($E_f$) or relative energies ($\Delta E_f$) and Boltzmann-weighted relative populations at catalytically relevant temperature of 1000 K. Point-group symmetry and spin multiplicities are shown in red. Point group symmetry was assigned by inspection; multiplicities and energies were calculated from Quantum Espresso.

where $E_{\mathrm{cluster}}$ is the total DFT energy of the cluster, $E[\mathrm{Pd}_1(\mathrm{Pt}_1)]$ is the DFT energy of a Pd(Pt) atom, and $N_{\mathrm{Pd(Pt)}}$ is the number of Pd(Pt) atoms composing the cluster. The Boltzmann probability (for a given Pt/Pd ratio) for $i$-th configuration ($P_i$) was found by taking the Boltzmann distribution of each minimum ($e^{-E_i/k_BT}$) divided by the sum of the distributions of all relevant low energy minima:

**Table 1. DFT Formation Energies ($E_f$) of the Gas-Phase Structures and their Boltzmann Populations at 700 K and 1000 K**

| no. Pd | no. Pt | $E_f$ tetrahedral (eV) | $P_{700\ K}$ | $P_{1000\ K}$ | $E_f$ planar (eV) | $P_{700\ K}$ | $P_{1000\ K}$ |
|---|---|---|---|---|---|---|---|
| 0 | 4 | −11.89 | 97.49% | 92.84% | −11.67 | 2.51% | 7.16% |
| 1 | 3 | −9.68 | 99.93% | 99.41% | −9.24 | 0.07% | 0.59% |
| 2 | 2 | −8.81 | 100.00% | 99.91% | −8.17[a] | <0.01% | 0.06% |
|  |  |  |  |  | −8.10[b] | <0.01% | 0.03% |
| 3 | 1 | −7.84 | 100.00% | 99.99% | −7.07 | <0.01% | 0.01% |
| 4 | 0 | −6.65 | 100.00% | 99.99% | −5.85 | <0.01% | 0.01% |

[a]. Pd−Pd−Pt−Pt planar structure, which is bilaterally symmetric through the plane bisecting the edge of the square planar structure. [b]. Pd−Pt−Pd−Pt planar structure, which is bilaterally symmetric through the plane bisecting the diagonal of the square planar structure.

$$P_i = \frac{e^{-E_i/k_BT}}{\sum e^{-E_i/k_BT}}$$

Here, $E_i$ is the $i$-th configuration energy of a cluster (i.e., $E_{\mathrm{cluster}}$ as defined above).

In Table 1 and Figure 1, only the relevant local minima are shown, and although other local minima were found, their relative probability fractions were negligible—that is, below the level of a part in $10^3$. It is noted that all global minima for the tetramers had a tetrahedral geometry, but this is often not the case for the supported clusters, discussed below. At 1000 K, a 0.44 eV difference between the tetrahedral and planar structures of $\mathrm{PdPt_3}$ translates to 99.41% of the cluster adopting the tetrahedral geometry in the gas phase. Differences in formation energies greater than 0.44 eV would only serve to underline the dominance of tetrahedra in the gas phase (see Table 1 and Figure 1).

**Table 2. Calculated Adsorption Energies ($E_{\mathrm{ads}}$) and Sintering Energy Penalties ($E_s$) of Global Minima of Adsorbed Clusters**

| no. Pd | no. Pt | geometry | $E_{\mathrm{ads}}$ (eV) | $E_s$−Pt (eV) | $E_s$−Pd (eV) |
|---|---|---|---|---|---|
| 0 | 4 | square planar | −4.08 | 2.20 |  |
| 1 | 3 | square planar | −3.67 | 2.13 | 1.67 |
| 2 | 2 | tetrahedron | −3.34 | 2.23 | 1.67 |
| 3 | 1 | tetrahedron | −2.88 | 2.17 | 1.53 |
| 4 | 0 | square planar | −2.64 |  | 1.47 |

**3.2. Clusters Deposited on $\mathrm{TiO_2}$(110).** In Tables 2 and 3, the adsorption energies ($E_{\mathrm{ads}}$) for a given cluster are given by

$$E_{\mathrm{ads}}[\mathrm{Pt}_m\mathrm{Pd}_n] = E[\mathrm{Surf} + \mathrm{Pt}_m\mathrm{Pd}_n] - E[\mathrm{Surf}] - E_{\mathrm{gas,min}}[\mathrm{Pt}_m\mathrm{Pd}_n]$$

where $E$ [Surf + $\mathrm{Pt}_m\mathrm{Pd}_n$] is the total DFT energy of the supported cluster system, $E$[Surf] is the total energy of the bare support, and $E_{\mathrm{gas,min}}[\mathrm{Pt}_m\mathrm{Pd}_n]$ is the global minimum of the gas-phase cluster. Table 2 lists the adsorption energies of the global minima of adsorbed clusters at varying ratios of Pt/Pd, as well as the sintering energy penalty (the energy cost of an atom of a given element to break away from a tetramer) forming a trimer and a monomer on the support:

$$E_s[\mathrm{Pt}_m\mathrm{Pd}_n - \mathrm{Pt}] = E[\mathrm{Surf} + \mathrm{Pt}_{m-1}\mathrm{Pd}_n] + E[\mathrm{Surf} + \mathrm{Pt}_1] - E[\mathrm{Surf} + \mathrm{Pt}_m\mathrm{Pd}_n] - E[\mathrm{Surf}]$$

if a Pt atom is "de-sintering," or

$$E_s[\mathrm{Pt}_m\mathrm{Pd}_n - \mathrm{Pd}] = E[\mathrm{Surf} + \mathrm{Pt}_m\mathrm{Pd}_{n-1}] + E[\mathrm{Surf} + \mathrm{Pd}_1] - E[\mathrm{Surf} + \mathrm{Pt}_m\mathrm{Pd}_n] - E[\mathrm{Surf}]$$

if a Pd atom is dissociating. It is emphasized that for the data in Table 2, all DFT energies used are of global minima, but this was not the case for the Metropolis MC where Boltzmann weighted averages of the energies were employed.

Table 3 presents the relative adsorption energies ($\Delta E_{\mathrm{ads}}$) of local minima ($E_{\mathrm{ads}}[\mathrm{Pt}_m\mathrm{Pd}_n]$) with respect to the global minimum, as well as Boltzmann probabilities ($P_I$) and Gibb's entropies ($S_G$). The $P_I$ are calculated in an analogous manner to the probabilities calculated for gas phase configurations, i.e.

$$P_I = \frac{e^{-E_I/k_BT}}{\sum e^{-E_I/k_BT}}$$

For the $I$-th adsorbed cluster, $E_I$ is the total energy of the adsorbed cluster on the support $E[\mathrm{Surf} + \mathrm{Pt}_m\mathrm{Pd}_n]$ and the partition function $(\sum e^{-E_I/k_BT})$ is the sum of the discrete configurational states listed in Table 3. The lowest minima are displayed in Figure 2 and all other local minima may be found in SI. A statistical definition of entropy utilizing the Boltzmann probabilities of these discrete states was applied to obtain the entropy ($S_G$) of the various cluster types given by

$$S_G = k_B \sum_I P_I \ln(P_I)$$

where the $P_I$ are the Boltzmann weights. In this way, the entropic contribution of the adsorbed clusters to the free energy of the system may be found. The fundamental thermodynamic relation of the Helmholtz free energy ($F = U - TS$) allows for the entropic energy contributions ($TS_G$) of the system, at the different ratios of Pt/Pd, to be accounted. It is noted that these entropic and probabilistic measures are defined in a canonical ensemble, wherein the partition function is defined by the sum of Boltzmann distributions of discretized states at varying ratios of Pt and Pd. The use of calculated or theoretical probabilities to define a discretized partition function in the canonical or microcanonical ensemble in order to derive free energies and entropies may be found in a number of other related works.[57−60]

This above analysis leads to a thermodynamic argument that suggests that a 1:1 mixture of Pt−Pd clusters is entropically favored as a result of the high number of thermally accessible isomers relative to those accessible to other clusters. Although the corresponding entropies reveal a fairly minute energetic contribution of 0.055 and 0.102 eV for 700 and 1000 K, respectively, such contributions can become more pronounced with increasing cluster size—i.e. such entropic contributions to the free energy may increase with the system size.

**3.3. Simulations of Cluster Sintering on the Support at Various Temperatures and Relative Concentrations.** Sintering simulation were carried out at 300 K, 700 K, and 1000 K, starting with the monomers strewn randomly on the support at 0.16 ML coverage, with Pd/Pt ratios of 1:3, 1:1, and 3:1.

Table 3. Relative Adsorption Energies ($\Delta E_{ads}$) and Boltzmann Probabilities ($P$) of Local Minima, and Entropic Energies (TS) at Catalytically Relevant Temperatures: 700, 1000 K

| no. Pd | no. Pt | isomer | geometry | $\Delta E_{ads}$ (eV) | $P$, 700 K | P, 1000 K | TS, 700 K (eV) | TS, 1000 K (eV) |
|---|---|---|---|---|---|---|---|---|
| 0 | 4 | I | square planar | 0.00 | 94.70% | 88.25% | 0.013 | 0.031 |
| | | II | tetrahedron | 0.17 | 5.30% | 11.73% | | |
| | | III | diamond | 0.55 | 0.001% | 0.021% | | |
| 1 | 3 | I | square planar | 0.00 | 86.46% | 74.84% | 0.030 | 0.064 |
| | | II | tetrahedron | 0.14 | 7.02% | 12.91% | | |
| | | III | tetrahedron | 0.19 | 6.52% | 12.25% | | |
| 2 | 2 | I | tetrahedron | 0.00 | 68.61% | 55.89% | 0.055 | 0.102 |
| | | II | square planar | 0.07 | 20.62% | 24.09% | | |
| | | III | tetrahedron | 0.15 | 5.28% | 9.28% | | |
| | | IV | square planar | 0.16 | 4.95% | 8.88% | | |
| | | V | tetrahedron | 0.29 | 0.54% | 1.87% | | |
| 3 | 1 | I | tetrahedron | 0.00 | 56.93% | 54.55% | 0.042 | 0.063 |
| | | II | tetrahedron | 0.02 | 42.99% | 44.82% | | |
| | | III | rhombus | 0.41 | 0.07% | 0.48% | | |
| | | IV | diamond | 0.51 | 0.01% | 0.15% | | |
| 4 | 0 | I | square planar | 0.00 | 70.40% | 64.71% | 0.037 | 0.056 |
| | | II | tetrahedron | 0.05 | 29.60% | 35.29% | | |

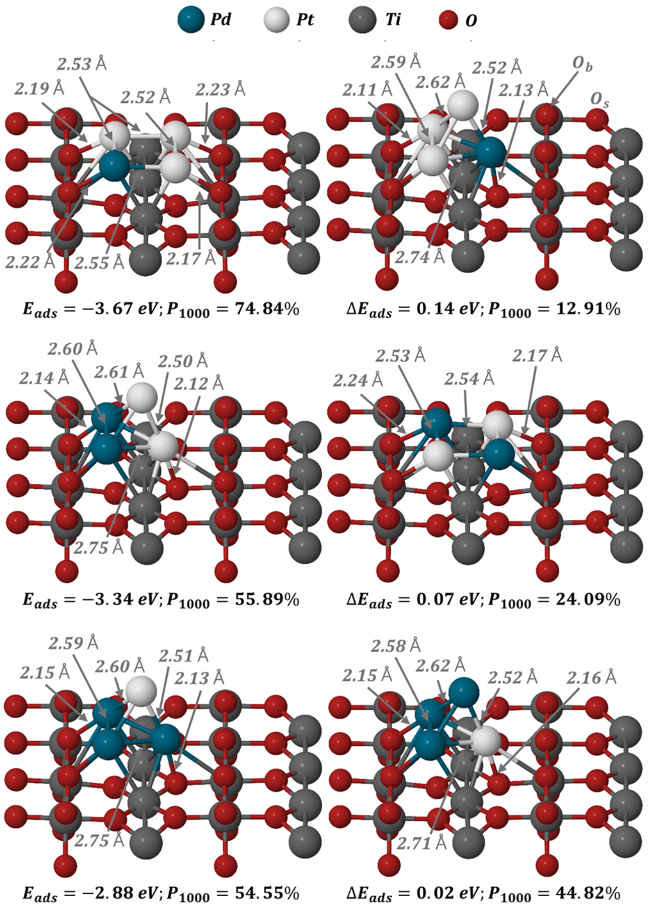

**Figure 2.** Global minimum and second lowest minimum of the mixed clusters once supported on rutile are displayed with their Boltzmann-weighted relative populations at 1000 K. In simulations of cluster sintering on the support, the experimentally relevant temperature range for clusters used in catalysis is from 700 to 1000 K. In this range, several low-energy isomers for supported clusters become relevant and thermally accessible. Only the adsorbed cluster and topmost layer of stoichiometric $TiO_2$ are visualized. Other local minima are visualized in SI.

Evaporation and redeposition of the monomers were allowed. However, no significant loss of the population was observed, consistent with the fairly deep and stabilizing minima on the PESs of the monomers moving on the support and visualized in Figure 3j,k. Results of these sintering simulations are shown in Figure 3a—i. An explanation of what is presented is the following: A given initial configuration ($C_i$) after a given number of Metropolis cycles ($M$) will have a "final" configurational state ($C_f$), wherein a certain fraction of the atoms ($F$) will be members of a particular cluster type ($Pt_mPd_n$). Given that $C_i$ is a stochastic variable, several different states can exist. If these were all allowed to evolve for, perhaps, billions of steps then all such configurations would end up with all atoms joined into one large cluster. By sampling over all pseudorandom configurations and averaging these atom-fractions for a particular $Pt_mPd_n$ over all $C_f$, an expectation value for the fraction of atoms belonging to a given $m$ and $n$ type cluster is acquired ($<F_{mn}>$), and an estimation of the stability of certain cluster types can be gained by looking at the distributions in Figure 3. For example, if the distributions were relatively flat, spread everywhere within the range of the given number of atoms in the simulation cell, this could indicate a very sensitive dependence on the initial configuration and/or that a great deal more cycles ($M$) are required. If the distribution was completely shifted to the larger clusters (limited to the number of atoms in the simulation space), then this would be an indication that the smaller clusters are easily "eaten" by larger ones, thus, sintering is not suppressed. Tight distributions near the origin imply that the system is relatively resistant to sintering.

Assessments of the stability of certain cluster types can be gained by looking at the distributions in Figure 3. The data represent the average cluster size and composition distributions of 1000 independent random initial configurations at a given temperature and Pt/Pd molar fraction after each has been run for more than 10 000 000 MC steps. Again, the plots do not represent true final-state distributions, because the final state of a system subject to Ostwald ripening will always result in a single large island of all the deposited atoms on the support. More interesting are the trends in cluster size evolution as the temperature increases and the Pt content varies.

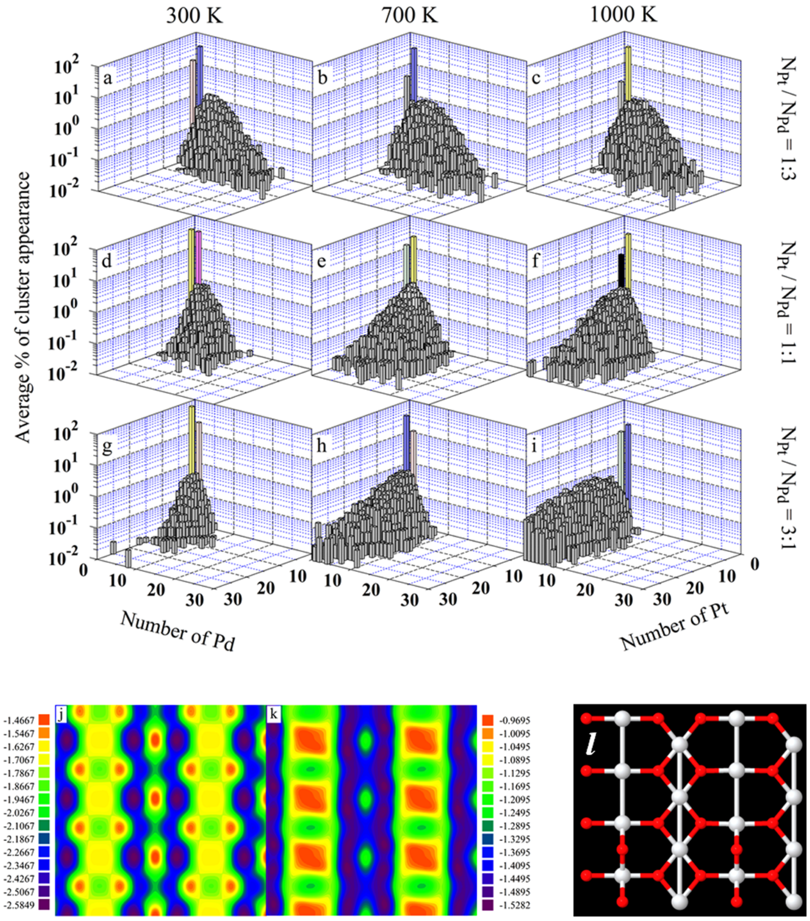

**Figure 3.** Results of sintering simulations (10,000,000 steps) at 300 K (a,d,g), 700 K (b,e,h), 1000 K (c,f,i) and compositions of the initial mixtures of the monomers for Pt/Pd ratio of 1:3 (a,b,c), Pt/Pd ratio of 1:1 (d,e,f), Pt/Pd ratio of 3:1 (g,h,i). Parts (j) and (k) show the PES for the Pt and Pd monomers, respectively; scales show the adsorption energy in eV; the locations of the underlying surface atoms are illustrated in (l).

The distributions that are tightest with peaks near the origin are those at 300 K with initial Pt concentrations of 50% or greater, Figure 3(d,g). At Pt/Pd ratios of 1:3, there is evidence showing that some of the initial configurations evolved to relatively large clusters within the given number of Metropolis cycles. This implies that conditions of 50% or greater initial Pt concentrations lead to good cluster stability as the monomers do not all rapidly evolve into a single large island (from classical transition state theory, it is predicted here that tetramers form within a fraction of a second). Figure 3(a—c) show that high concentrations of Pd generally leads to relatively poor stability for small subnanoclusters at all temperatures. It is noted that at 300 K, a clear peak for small $Pd_n$ clusters is present; one of these clusters is $Pd_4$. This cluster was previously explored and found to exhibit a good matching with the underlying surface oxygen atoms and stabilizing $\sigma$-aromatic character of chemical bonding within the cluster.[52] However, at temperatures relevant to the industrial use of Pt—Pd clusters in catalysis (i.e., 700 to 1000 K), the systems “boil” out of this minimum and move away from the *Y*-axis (labeled by the number of Pd) toward the diagonal of the XY plane, corresponding to 1:1 mixtures—Figure 3b,c. Also at higher temperatures, it is shown that having 50% or less Pt improves the stability of small clusters, as can be seen in Figure 3c,f,i, where 1:3 and 1:1 distributions are tighter than 3:1. There is a hint that perhaps at very high temperatures an ideal initial Pt concentration may be somewhere around 35—40%. To determine this would require a more detailed study using DFT and/or MD to model clusters composed of several tens of atoms or more; this is beyond the scope of the present work.

From Figure 3, it is argued that there is a general preference for roughly equimolar clusters as the tightest distributions and most clearly defined peaks close to the origin are those belonging to such, of heavier populations of the clusters with one dominant component also being obvious when the starting monomer distribution is unequal. However, there are indications that the 1:1 ratio leads to more sintering resistant clusters for reasons noted above. This result is also intuitive based on the higher sintering energy penalties of the 1:1 tetramers (Table 2). Thus, the experimental observation that equimolar Pt—Pd clusters are more stable against sintering on the support than clusters of vastly different compositions is generally reproduced.

### 3.4. Explanations for the Preference for a 1:1 Phase.

Sintering simulations have primarily confirmed the experimental result for a preference of equimolar clusters. Therefore, it is natural to suspect that there must be something unique about the geometric and electronic structures of these clusters. Several forms of chemical bonding analyses were performed to address this question. In general, as will be shown, there exists a competition between maximized binding to the surface O atoms (favoring flat structures) and the intracluster bonding, i.e. delocalized overlap (favoring more compact 3D structures).

*3.4.1. Projected Density of States.* The projected density of states (PDOS) of Pd−O/Pt−O coordination and Pd−Pt coordination was extracted in order to compare density of states overlap of cluster−support against that of intracluster bonding. In PDOS analysis, the intensity and broadness of the peaks of the PDOS represent the distribution of electrons within atomic orbitals.[61] Favorable orbital mixing between two atoms arises when there is optimal overlap between their respective PDOS.[62]

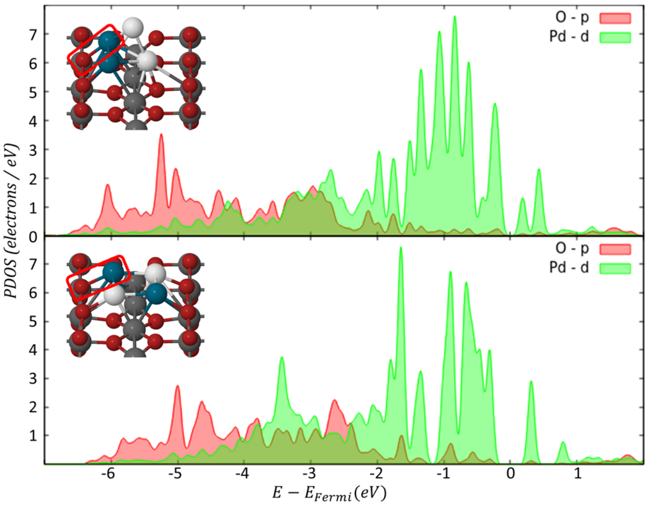

**Figure 4.** Projected density of states of Pd coordinated to $O_b$. (Top) The global minimum of $Pd_2Pt_2$, a tetrahedron. (Bottom) The second lowest minimum of $Pd_2Pt_2$, square planar.

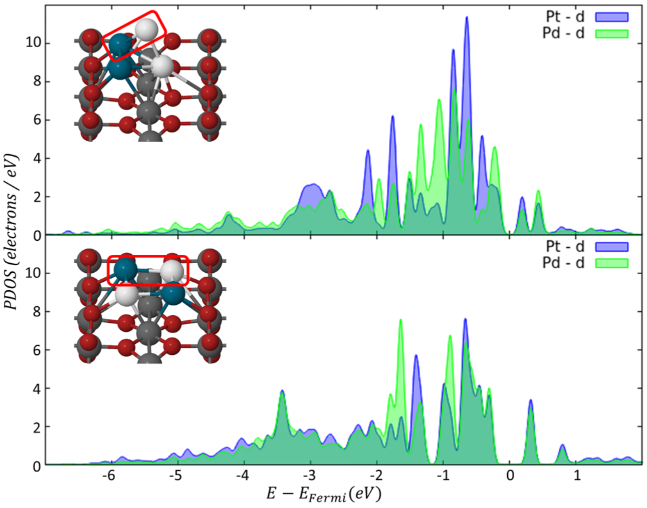

**Figure 5.** Projected density of states of Pd coordinated to Pt. (Top) $Pd-Pt_{apex}$ of the global minimum of $Pd_2Pt_2$, a tetrahedron. (Bottom) Pd−Pt (symmetric to the other half of the structure) of the second lowest minimum of $Pd_2Pt_2$, square planar.

In Figures 4 and 5, only the energy ranges for integration of valence electrons were visualized: Figure 4 is focused on cluster-support interactions and Figure 5 on intracluster bonding. Only d projections are visualized as integration of s and p PDOS yielded small fractional contributions (s-electrons are also addressed separately in the following section). Optimal p−d mixing occurs between cluster-O in the range of −6 to −2 eV, while intense d−d mixing occurs between cluster atoms in the range of −2 eV up to the Fermi energy, which is set at 0 for ease of visualization. The distribution between these two ranges reveals the unique bonding environment for one structure over the other.

Integration of the PDOS in s, p, and d distributions reveals Pt's approximately equal distribution of five electrons for cluster-support interaction and five electrons for the high intensity peaks of d−d mixing in intracluster bonding; Pd's differs slightly with four and six, respectively. A similar trend takes place in planar $Pt_3Pd$ and explains in part the predominance of 2D over 3D as Pt favors covalent Pt−O bonds. Due to the symmetric electronic environment of planar $Pd_2Pt_2$, Pd−Pd, and Pt−Pt s, p, and d distributions overlap completely and Pt−Pd overlap nearly perfectly.

In contrast, the 50/50 global minimum, a tetrahedron, exhibits a more uneven distribution although a similar p−d mixing trend may be observed in Figure 4. The tetrahedron's triangular base features 2 $Pd-O_b$ coordination and 1 $Pt-O_s$ coordination ($O_b$, $O_s$ are labeled in Figure 2). The two basal Pd and the apical Pt illustrate a preference for d−d mixing, Pd conserving six electrons for high intensity d−d mixing and four electrons for $Pd-O_b$ coordination and Pt reserving six electrons within the high intensity range and four electrons in the delocalized ranges of −6 to −2 eV. The basal Pt preferentially delocalizes seven electrons in the lower energy range of −2 eV and below for optimal $Pt-O_s$ coordination and compensation for Pd d−d mixing where the apical Pt distribution falls; only three electrons fall in the maximum d−d peak range of −2 eV to the Fermi energy. This trend repeats in $Pd_3Pt$ tetrahedra and contributes to the predominance of 3D over 2D as Pd favors d−d mixing over $Pd-O_b$ coordination.

In general, in binding to surface oxygen atoms, 2D clusters are favored. They lay flat and wet the support, maximizing the number of interactions with surface O atoms, and exhibit a significant degree of covalency in these bonds. The 3D structures also coordinate with surface O atoms, but these interactions are compromised due to poor geometric matching with the interface. In terms of binding to the support, pure and mixed clusters show some difference due to the relative electronegativities of Pt, Pd, and O, where the degree of charge transfer to the support and the resultant ionic component are mildly affected—discussed further in subsection 3.4.3. Intracluster bonding is analyzed next, from a molecular orbital (MO) picture.

*3.4.2. Intracluster and Cluster−Support Bonding.* Intracluster bonding is also similar between all considered tetramers, as the basic bonding principle is the same for the 2D and 3D structures. The Pd and Pt atoms in isolation have the electronic configuration of $[RG]d^{10}s^0$ and $[RG]d^9s^1$, respectively, which renders them rather inert. When four atoms come together to form a cluster, the four sets of valence d- and s-AOs form a total of 24 MOs being populated by 40 electrons. Population of the MOs originates from the valence s-AOs as required for the clusters to be bound. In the case of pure Pd clusters, the MOs formed by d- and s-AOs completely separate. By inspection, it is found that only one MO originating from s-AOs is populated for the square-planar global minimum; it is delocalized and completely symmetric; it is a $\sigma$-MO. Starting from the $Pd_4$ cluster being populated by two electrons, this $\sigma$-MO makes the cluster obeys the $(4n + 2)$ Hückel's rule with $n = 0$ for aromatic species, hence, $Pd_4$ is $\sigma$-aromatic.[51,63−65] Aromaticity can be 2D (as in the planar) or 3D (as in the tetrahedral, see SI for gas-phase results). The two-electron hole left in the d-set in $Pd_4$

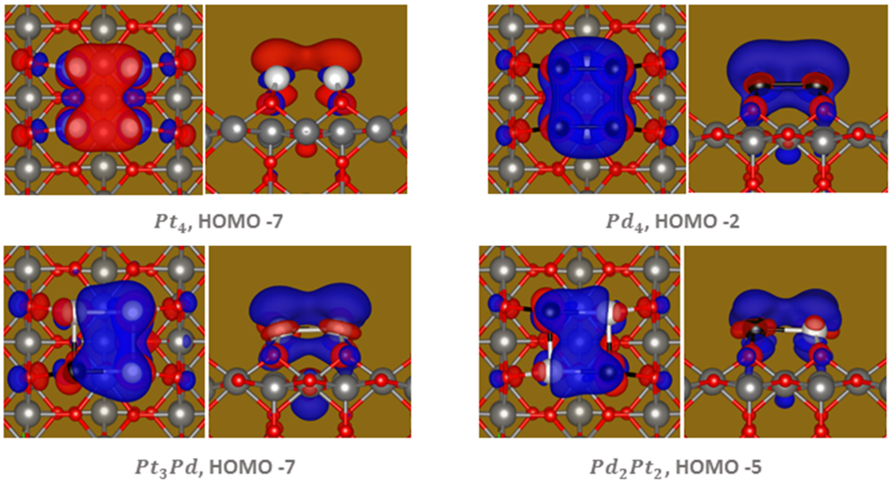

$Pt_4$, HOMO -7

$Pd_4$, HOMO -2

$Pt_3Pd$, HOMO -7

$Pd_2Pt_2$, HOMO -5

**Figure 6.** s-MOs formed by s-AOs of pure (top) and mixed (bottom) planar clusters. MOs are not separable from the d-states. For clarity, Pt is white, Pd is black, Ti is dark gray, and O is red.

also contributes to the net-bonding effect.[51] This is relevant as aromaticity is a chemically stabilizing effect.[66]

The $\sigma$-MOs formed by s-AOs are easily distinguishable in planar adsorbed clusters (Figure 6). In 3D adsorbed clusters, the $\sigma$-bonding overlap is stronger as the corresponding MO goes deeper in the valence set, mixes with the MOs formed by d-AOs, and becomes indistinguishable. In 2D species, $\sigma$-states are energy-separated from d-states and can be easily found by inspection, but the 3D species require an alternative mode of analysis such as projected DOS to recognize the same bonding pattern. The previous section examined in detail the delocalized chemical bonding present in tetrahedral clusters and determined Pd's preference toward d−d mixing and Pt's preference toward p−d mixing with coordinating O. An analogous shift in electron density may be found in the extracted $\sigma$-MOs of the planar clusters.

Thus, the chemical bonding in all studied clusters is delocalized, and may be qualified as $\sigma$-aromatic. It is also important to note that the delocalized overlap is optimal when the cluster is most compact (i.e., 3D and not 2D). Therefore, the intracluster bonding overlap is more pronounced in tetrahedral clusters rather than planar clusters. This contributes to the dominance of tetrahedral over planar gas-phase clusters (see SI). Hence, for clusters on the support, binding to surface oxygen favors planar structures and intracluster bonding favors tetrahedral structures, and as a result, the two forms are very close in energy. In STEM images of larger nanoparticles,[15] 3D species prevail; ultimately, intracluster bonding dominates.

Importantly, the difference in the electron constitution of Pt−Pd clusters of all compositions is small; metal substitution has very little effect on the nature and the population of valence MOs in these systems. Given that the bonding is very similar, it cannot be the major culprit for the stability of the 1:1 clusters.

*3.4.3. Charging and Electrostatics.* The small difference between electonegativities of Pt and Pd (respectively 2.28 and 2.20) leads to the Pt atoms becoming slightly negatively charged; all Pd atoms becoming slightly positive. Due to charge-separation, there is an additional electrostatic contribution to the binding in mixed clusters. It was hypothesized that the Coulomb potential, $V_C = (\sum q_i q_j / r_{ij})$, between these partial charges would lead to an additional stabilization, favoring the 1:1 mixtures. Table 4 shows the value of the Coulomb potential of the given cluster in gas phase and the Boltzmann-weighted average Coulomb potential (using weights from Table 1). It was found that when compared to the gas-phase clusters—wherein all clusters are neutral—the adsorbed clusters undergo a modest charge transfer from the cluster to the support, as a result of the more electronegative O atoms. Table 5 summarizes the electrostatic results for the global and local minima of adsorbed clusters. Charges of planar structures range from 0.32 to 0.44 e, and the tetrahedra range from 0.21 to 0.34 e (see Table 5). The net charge on the cluster indicates that during adsorption charge transfer has taken place from the cluster to the $TiO_2(110)$ surface.

**Table 4. Coulomb Potential ($V_C$) of Gas-Phase Clusters[a,b]**

| no. Pd | no. Pt | $V_C$ tetrahedral (eV) | $V_C$ planar (eV) | $\Sigma P_i V_{Ci}$ 1000 K (eV) |
|---|---|---|---|---|
| 0 | 4 | −0.01 | −0.12 | −0.02 |
| 1 | 3 | −0.10 | −0.23 | −0.10 |
| 2 | 2 | −0.15 | −0.08[c]<br>−0.25[d] | −0.15 |
| 3 | 1 | −0.11 | −0.14 | −0.11 |
| 4 | 0 | −0.01 | −0.05 | −0.01 |

[a] Partial charges were summed for all gas-phase structures to confirm the neutrality of the cluster. [b] In gas-phase clusters, the global minimum is always tetrahedral. [c] Pd−Pd−Pt−Pt planar structure, which is bilaterally symmetric through the plane bisecting the edge of the square planar structure. [d] Pd−Pt−Pd−Pt planar structure, which is bilaterally symmetric through the plane bisecting the diagonal of the square planar structure.

All gas-phase clusters are electrostatically stabilized, as is shown in Table 4. Overall, the planar structure has greater electrostatic stability with the Coulomb potential of the lowest energy planar isomer being roughly double that of the lowest energy tetrahedral structure and, for the case of the pure tetramer, an order of magnitude greater (there is a small charge separation even in monometallic clusters). Pure Pd and Pt clusters exhibit the weakest electrostatic stabilization and 1:1 ratios the strongest for all gas-phase structures. A reversal in the trend of electrostatic stabilization occurs between 2D and 3D structures going from the gas phase to adsorption.

For adsorbed clusters, charge separation decreases in the 2D and increases in the 3D. This results in the electrostatically destabilization of planar structures in favor of 1:1 Pd−O or Pt−O coordination, whose net repulsion (0.15 to 0.36 eV) among mixed clusters is compensated by consistently higher partial

Table 5. Charges ($Q$) and Coulomb Potentials ($V_{Ci}$) of Local Minima and Weighted Average Coulomb Potential for Accessible Isomers ($\Sigma P_i V_{Ci}$)

| no. Pd | no. Pt | isomer | geometry | Q (e) | $V_{Ci}$ (eV) | $\Sigma P_i V_{Ci}$ 700 K (eV) | $\Sigma P_i V_{Ci}$ 1000 K (eV) |
|---|---|---|---|---|---|---|---|
| 0 | 4 | I | square planar | 0.28 | −0.13 | 0.08 | 0.06 |
| | | II | tetrahedron | 0.20 | 0.09 | | |
| | | III | diamond | 0.22 | −1.16 | | |
| 1 | 3 | I | square planar | 0.32 | 0.15 | 0.12 | 0.09 |
| | | II | tetrahedron | 0.25 | −0.21 | | |
| | | III | tetrahedron | 0.21 | 0.07 | | |
| 2 | 2 | I | tetrahedron | 0.28 | −0.41 | −0.25 | −0.20 |
| | | II | square planar | 0.36 | 0.16 | | |
| | | III | tetrahedron | 0.29 | −0.27 | | |
| | | IV | square planar | 0.36 | 0.21 | | |
| | | V | tetrahedron | 0.27 | 0.04 | | |
| 3 | 1 | I | tetrahedron | 0.32 | −0.30 | −0.22 | −0.21 |
| | | II | tetrahedron | 0.29 | −0.11 | | |
| | | III | rhombus | 0.38 | −0.09 | | |
| | | IV | diamond | 0.43 | −0.88 | | |
| 4 | 0 | I | square planar | 0.44 | 0.33 | 0.26 | 0.25 |
| | | II | tetrahedron | 0.34 | 0.35 | | |

positive charges as compared to tetrahedra. Mixed 3D structures are electrostatically stabilized due to the increase in charge separation between Pt and Pd with a net intracluster attraction on the order of a few tenths of an eV, for example, from Table 5: $Pd_3Pt$-Isomer I and II, $Pd_2Pt_2$—Isomer I, and $PdPt_3$—Isomer II. In such clusters, where the global minimum is a tetrahedron, the apex is always Pt, whose negative partial charge almost doubles when compared with the gas-phase cluster. Thus, an electrostatic sandwiching effect occurs with the tetrahedron's positive base interleaved between the negative apex and the electronegative surface oxygens. This explains the dominance of $Pd_3Pt$ tetrahedra over their planar counterpart because the tetrahedra can maximize this electrostatic binding with an electropositive $Pd_3$ base (Isomer I) or $Pd_2Pt$ base (Isomer II).

Just as 50/50 ratios of Pd and Pt in the gas phase demonstrated the greatest electrostatic stability, 50/50 ratios of Pd and Pt adsorbed to the surface attain the optimal balance between surface-cluster coordination and intracluster attraction. The global minimum of $Pd_2Pt_2$, a tetrahedron, has the greatest electrostatic stability at −0.41 eV and one of the highest induced charges among 3D structures (0.28 e). The next local minimum, a planar structure, acquires the greatest charge among mixed clusters at 0.36 e, but also one of the highest intracluster Coulomb repulsions of 0.16 eV, second only to pure $Pd_4$ and comparable to $Pt_3Pd$. By Boltzmann-averaging the Coulomb potentials, an estimate can be gained for the net electrostatic interaction within a particular tetramer type. When this is done, only the 1:1 and 1:3 Pt to Pd structures possess an overall Coulombic stabilization. However, the 1:3 Pt to Pd structures exhibit distorted planar structures of a rhombus and diamond, which display minimal coordination to the surface (see SI) in contrast to their high positive partial charges (0.38 and 0.44 e) and calculated electrostatic stabilization (−0.09 and −0.88 eV). The nonappearance of Pd-rich phases in experiments could be due to such phases becoming oxygenated before sintering to large nanoparticles, coupled with the fact that Pd more readily dissociates from Pd-rich clusters relative to other fragmentation processes (see Table 2).

To estimate the contribution of the Coulomb interaction as a function of cluster growth, solid-state calculations were carried out on several unit cells of various composition of Pt and Pd. Table 6 summarizes the results for several mixed lattices, showing the Strukturbericht label, the cohesive energy ($E_{coh}$), the optimized lattice constant ($a_{lat}$), and the percent of the Ewald contribution to the total DFT energy—it is noted that all Ewald contributions are attractive. Calculations are in reasonable agreement with other theoretical results.[67]

Table 6. Cohesive Energy ($E_{coh}$), Lattice Constant ($a_{lat}$), and Percent of Ewald to DFT energy for Several Unit Cells of Various Compositions of Pt and Pd

| Strukturbericht Pt/Pd | $E_{coh}$ (eV/atom) | $a_{lat}$ (Å) | $V_{Ewald}/V_{DFT}$ (%) |
|---|---|---|---|
| $L1_2$ 3:1 | −5.60 | 3.97 | 66.42 |
| $L1_0$ 1:1 | −5.01 | 3.98<br>3.90 | 68.39 |
| B2 1:1 | −4.99 | 3.13 | 73.34 |
| B1 1:1 | −4.26 | 5.28 | 67.96 |
| $L1_2$ 1:3 | −4.40 | 3.94 | 75.78 |

The Pt dominant unit cell is the most stable from the magnitude of $E_{coh}$, two structures of the 1:1 lattices follow behind and are very close in energy (a fcc-like $L1_0$ structure and a CsCl-like B2 structure), differing by 0.02 eV. The 1:1 mixtures have a slightly larger Ewald contribution than the 3:1 (Pt/Pd) lattice, but smaller than that of the 1:3 lattice, which itself is overall the most weakly bound. The results suggest that electrostatic stabilization does play an important role as the clusters sinter to larger nanoparticles and acquire more bulk-like properties.

## 4. CONCLUSIONS

An in-depth theoretical study of sintering of mixed Pt—Pd clusters on $TiO_2(110)$ was presented. Our in-house ab initio Monte Carlo algorithm simulates the process of Ostwald ripening, including cluster dissociation and formation through the exchange of monomers, as well as monomer evaporation from the support and coverage-dependent redeposition. The evolution of cluster size and composition distributions at experimentally relevant temperatures was modeled. In agreement with earlier observations, the 1:1 clusters are relatively favored at relevant temperatures. Further structural and chemical bonding analyses revealed no obvious reason for favoring the equally mixed clusters. One subtle difference that was shown to lead to a unique stability was electrostatic stabilization within the cluster. Charge redistribution, from Pd to Pt, results in an intracluster Coulomb interaction. This interaction was shown to be the most favorable for clusters containing Pt and Pd in equal proportions. In addition, the 50/50 mixtures were shown to have considerably more thermally relevant isomers at higher temperatures than clusters of any other compositions. As a result, there is a configurational entropic stabilization, which is smaller than the electrostatic effect. Both the entropic and Coulombic stabilization can be enhanced as the clusters grow larger. Thus, a well-motivated hypothesis was presented to explain why at catalytically relevant temperatures, small Pt−Pd nanoparticles of roughly 1:1 concentration are the most resistant to sintering.

This study sites two subtle but apparently critical effects leading to stabilization of deposited clusters against sintering: entropic and electrostatic. It is likely that such effects may govern the stability of other bi- and poly-metallic deposited clusters.

## ASSOCIATED CONTENT

### Supporting Information

Ab initio calculation of Pt−Pd clusters. Dimers and trimers of mixed Pt−Pd clusters.This material is available free of charge via the Internet at http://pubs.acs.org.

## AUTHOR INFORMATION

### Corresponding Author

*E-mail: ana@chem.ucla.edu.

### Author Contributions

§M.-A.H. and J.D. contributed equally to this work.

### Notes

The authors declare no competing financial interest.

## ACKNOWLEDGMENTS

This material is based in part on work supported by the Air Force Office of Scientific Research (AFOSR) under grant number, 10029173-S3. ANA also thanks the Alfred P. Sloan Foundation Fellowship. Computational resources were provided by the UCLA-IDRE cluster. A portion of the research was performed using EMSL, a national scientific user facility sponsored by the Department of Energy's Office of Biological and Environmental Research and located at Pacific Northwest National Laboratory. J.D. acknowledges a number of important conversations with Dr. Jin Zhang. The Authors also thank Professor William Gelbart for a useful discussion.

## REFERENCES

(1) Bhasin, M.; McCain, J.; Vora, B.; Imai, T.; Pujado, P. *Appl. Catal., A* **2001**, *221*, 397−419.

(2) Galvita, V.; Siddiqi, G.; Sun, P.; Bell, A. *J. Catal.* **2010**, *271*, 209−219.

(3) Burch, R.; Garla, L. *J. Catal.* **1981**, *71*, 360−372.

(4) Weckhuysen, B.; Schoonheydt, R. *Catal. Today* **1999**, *51*, 223−232.

(5) Kim, J.; Park, S.; Chun, B.-H.; Jeong, B.; Han, J.; Kim, S. *Catal. Today* **2012**, *185*, 47−53.

(6) Zhao, H.-L.; Meng, F.-X.; Guo, W.; Zou, J.-J.; Zhang, X.-W. *J. Fuel Chem. Technol.* **2008**, *36*, 462−467.

(7) Bariås, O.; Holmen, A.; Blekkan, E. *J. Catal.* **1996**, *158*, 1−12.

(8) Jablonski, E.; Castro, A.; Scelza, O.; de Miguel, S. *Appl. Catal., A* **1999**, *183*, 189−198.

(9) Sun, P.; Siddiqi, G.; Vining, W.; Chi, M.; Bell, A. *J. Catal.* **2011**, *282*, 165−174.

(10) Siddiqi, G.; Sun, P.; Galvita, V.; Bell, A. *J. Catal.* **2010**, *274*, 200−206.

(11) Ren, H.; Humbert, M.; Menning, C.; Chen, J.; Shu, Y.; Singh, U.; Cheng, W. *Appl. Catal., A* **2010**, *375*, 303−309.

(12) Jovanovic, M.; Putanov, P. *Appl. Catal., A.* **1997**, *159*, 1−7.

(13) Gutiérrez, A.; Arandes, J.; Castaño, P.; Aguayo, A.; Bilbao, J. *Energy Fuels* **2011**, *25*, 3389−3399.

(14) Graham, G.; Jen, H.-W.; Ezekoye, O.; Kudla, R.; Chun, W.; Pan, X.; McCabe, R. *Catal. Lett.* **2007**, *116*, 1−8.

(15) Johns, T.; Gaudet, J.; Peterson, E.; Miller, J.; Stach, E.; Kim, C.; Balogh, M.; Datye, A. *ChemCatChem* **2013**, *5*, 2636−2645.

(16) Anderson, R.; Zhang, L.; Loussaert, J.; Frenkel, A.; Henkelman, G.; Crooks, R. *ACS Nano* **2013**, *7*, 9345−9353.

(17) Henrich, V.; Cox, P. *The Surface Science of Metal Oxides*; Cambridge University Press, Cambridge, England, 1996.

(18) Henry, C. *Surf. Sci. Rep.* **1998**, *31*, 231−325.

(19) Diebold, U. *Surf. Sci. Rep.* **2003**, *48*, 53−229.

(20) Zhang, J.; Alexandrova, A. *J. Chem. Phys.* **2011**, *135*, 174702.

(21) Hansen, T.; DeLaRiva, A.; Challa, S.; Datye, A. *Acc. Chem. Res.* **2013**, *46*, 1720−1730.

(22) Giannozzi, P.; Baroni, S.; Bonini, N.; Calandra, M.; Car, R.; Cavazzoni, C.; Ceresoli, D.; Chiarotti, G.; Cococcioni, M.; Dabo, I.; Dal Corso, A.; Fabris, S.; Fratesi, G.; Gebauer, R.; Gerstmann, U.; Gougoussis, C.; Kokalj, A.; Lazzeri, M.; Martin-Samos, L.; Marzari, N.; Mauri, F.; Mazzarello, R.; Paolini, S.; Pasquarello, A.; Paulatto, L.; Sbraccia, C.; Scandolo, S.; Sclauzero, G.; Seitsonen, A.; Smogunov, A.; Umari, P.; Wentzcovitch, R. *J. Phys.: Condens. Mater.* **2009**, *21*, 395502.

(23) Kohn, W.; Sham, L. *Phys. Rev.* **1965**, *140*, A1133−A1138.

(24) Lee, C.; Yang, W.; Parr, R. *Phys. Rev. B* **1988**, *37*, 785−789.

(25) Burke, K.; Werschnik, J.; Gross, E. *J. Chem. Phys.* **2005**, *123*, 062206.

(26) Perdew, J.; Burke, K.; Ernzerhof, M. *Phys. Rev. Lett.* **1996**, *77*, 3865−3868.

(27) Kowalski, P.; Meyer, B.; Marx, D. *Phys. Rev. B* **2009**, *79*, 115410.

(28) Kowalski, P.; Camellone, M.; Nair, N.; Meyer, B.; Marx, D. *Phys. Rev. Lett.* **2010**, *105*, 146405.

(29) Tao, J.; Perdew, J.; Staroverov, V.; Scuseria, G. *Phys. Rev. Lett.* **2003**, *91*, 146401.

(30) Peterson, K.; Puzzarini, C. *Theor. Chem. Acc.* **2005**, *114*, 283−296.

(31) Figgen, D.; Rauhut, G.; Dolg, M.; Stoll, H. *Chem. Phys.* **2005**, *311*, 227−244.

(32) Hegarty, D.; Robb, M. *Mol. Phys.* **1979**, *38*, 1795−1812.

(33) Eade, R.; Robb, M. *Chem. Phys. Lett.* **1981**, *83*, 362−368.

(34) Schlegel, H.; Robb, M. *Chem. Phys. Lett.* **1982**, *93*, 43−46.

(35) Bernardi, F.; Bottoni, A.; Mcdouall, J.; Robb, M.; Schlegel, H. *Faraday Symp. Chem. Soc.* **1984**, *19*, 137−147.

(36) Frisch, M.; Ragazos, I.; Robb, M.; Schlegel, H. *Chem. Phys. Lett.* **1992**, *189*, 524−528.

(37) Yamamoto, N.; Vreven, T.; Robb, M.; Frisch, M.; Schlegel, H. *Chem. Phys. Lett.* **1996**, *250*, 373−378.

(38) Dunning, T.; Hay, P. *Modern Theoretical Chemistry*; Schaefer, H. F., III, Ed.; Plenum Press: New York, 1977; Vol. 3, pp 1−28.

(39) Hay, P.; Wadt, W. *J. Chem. Phys.* **1985**, *82*, 270−283.

(40) Wadt, W.; Hay, P. *J. Chem. Phys.* **1985**, *82*, 284−298.

(41) Hay, P.; Wadt, W. *J. Chem. Phys.* **1985**, *82*, 299−310.

(42) Frisch, M.; Trucks, G.; Schlegel, H.; Scuseria, G.; Robb, M.; Cheeseman, J.; Scalmani, G.; Barone, V.; Mennucci, B.; Petersson, G.; Nakatsuji, H.; Caricato, M.; Li, X.; Hratchian, H.; Izmaylov, A.; Bloino, J.; Zheng, G.; Sonnenberg, J.; Hada, M.; Ehara, M.; Toyota, K.; Fukuda, R.; Hasegawa, J.; Ishida, M.; Nakajima, T.; Honda, Y.; Kitao, O.; Nakai, H.; Vreven, T.; Montgomery,Jr., J.; Peralta, J.; Ogliaro, F.; Bearpark, M.; Heyd, J.; Brothers, E.; Kudin, K.; Staroverov, V.; Kobayashi, R.; Norm, J.; Raghavachari, K.; Rendell, A.; Burant, J.; Iyengar, S.; Tomasi, J.; Cossi, M.; Rega, N.; Millam, J.; Klene, M.;

Knox, J.; Cross, J.; Bakken, V.; Adamo, C.; Jaramillo, J.; Gomperts, R.; Stratmann, R.; Yazyev, O.; Austin, A.; Cammi, R.; Pomelli, C.; Ochterski, J.; Martin, R.; Morokuma, K.; Zakrzewski, V.; Voth, G.; Salvador, P.; Dannenberg, J.; Dapprich, S.; Daniels, A.; Farkas, Ö.; Foresman, J.; Ortiz, J.; Cioslowski, J.; Fox, D. *Gaussian 09* , revision D.01; Gaussian, Inc., Wallingford, CT, 2009.

(43) Tang, W.; Sanville, E.; Henkelman, G. *J. Phys.: Condens. Matter* **2009**, *21*, 084204.

(44) Sanville, E.; Kenny, S.; Smith, R.; Henkelman, G. *J. Comb. Chem.* **2007**, *28*, 899−908.

(45) Henkelman, G.; Arnaldsson, A.; Jonsson, H. *Comput. Mater. Sci.* **2006**, *36*, 354−360.

(46) Glendening, E.; Reed, A.; Carpenter, J.; Weinhold, F. *NBO*, version 3.1; University of Wisconsin, Theoretical Chemistry Institute: Madison, WI, 2005

(47) Metropolis, N.; Rosenbluth, A.; Rosenbluth, M.; Teller, A.; Teller, E. *J. Chem. Phys.* **1953**, *21*, 1087−1092.

(48) Hastings, W. *Biometrika* **1970**, *57*, 97−109.

(49) Wei, S.; Zeng, Z.; You, J.; Yan, X.; Gong, X. *J. Chem. Phys.* **2000**, *113*, 11127−11133.

(50) Addou, R.; Senftle, T.; O'Connor, N.; Janik, M.; van Duin, A.; Batzill, M. *ACS Nano* **2014**, *8*, 6321−6333.

(51) Zhang, J.; Alexandrova, A. *J. Phys. Chem. Lett.* **2012**, *3*, 751−754.

(52) Zhang, J.; Alexandrova, A. *J. Phys. Chem. Lett.* **2013**, *4*, 2250−2255.

(53) Kravitz, S. *Math. Mag.* **1967**, *40*, 65−71.

(54) Peikert, R.; Würtz, D.; Monagan, M.; de Groot, C. In *Proceedings of the Fifteenth IFIP Conference*, Zürich, Switzerland, September 2−6, 1991; Kall, P., Ed.; Springer-Verlag: Berlin, 1992; pp 45−54.

(55) Dart, F. *Phys. Rev.* **1950**, *78*, 761−764.

(56) Shen, L.; Dadras, J.; Alexandrova, A. *Phys. Chem. Chem. Phys.* **2014**, DOI: 10.1039/C4CP01877J.

(57) Wales, D.; Bogdan, T. *J. Phys. Chem. B* **2006**, *110*, 20765.

(58) Meng, G.; Arkus, M.; Brenner, M.; Manoharan, V. *Science* **2010**, *327*, 560−563.

(59) Oates, W.; Zhang, F.; Chen, S.-L.; Chang, Y. *Phys. Rev. B* **1999**, *59*, 11221.

(60) An, G. *J. Stat. Phys.* **1988**, *52*, 727−734.

(61) Hoffman, R. *Rev. Mod. Phys.* **1988**, *60*, 601−628.

(62) Carrasco, J.; Michaelides, A.; Scheffler, M. *J. Chem. Phys.* **2009**, *130*, 184707.

(63) Li, Z.; Moran, D.; Fan, K.; Schleyer, P. *J. Phys. Chem. A* **2005**, *109*, 3711−3716.

(64) Alexandrova, A.; Boldyrev, A. *J. Phys. Chem. A* **2003**, *107*, 554−560.

(65) Boldyrev, A.; Wang, L. *Chem. Rev.* **2005**, *105*, 3716−3757.

(66) Minkin, V.; Glukhovtsev, M.; Simkin, B. *Aromaticity and Antiaromaticity: Electronic and Structural Aspects*; John Wiley & Sons, Inc.: New York, 1994; p 313.

(67) Duan, Z.; Wang, G. *J. Phys.: Condens. Mater.* **2011**, *23*, 475301.